BNL-225822-2024-JAAM

GRP-COCAFP-11

Tandem Electrocatalytic-Thermocatalytic Conversion of CO2 to Aromatic Hydrocarbons

S. Garg, J. G. Chen

To be published in "ACS Energy Letters"

May 2024

Chemistry Department

Brookhaven National Laboratory

U.S. Department of Energy

USDOE Office of Science (SC), Basic Energy Sciences (BES)

Notice: This manuscript has been authored by employees of Brookhaven Science Associates, LLC under Contract No.DE-SC0012704 with the U.S. Department of Energy. The publisher by accepting the manuscript for publication acknowledges that the United States Government retains a non-exclusive, paid-up, irrevocable, world-wide license to publish or reproduce the published form of this manuscript, or allow others to do so, for United States Government purposes.

DISCLAIMER

This report was prepared as an account of work sponsored by an agency of the United States Government. Neither the United States Government nor any agency thereof, nor any of their employees, nor any of their contractors, subcontractors, or their employees, makes any warranty, express or implied, or assumes any legal liability or responsibility for the accuracy, completeness, or any third party's use or the results of such use of any information, apparatus, product, or process disclosed, or represents that its use would not infringe privately owned rights. Reference herein to any specific commercial product, process, or service by trade name, trademark, manufacturer, or otherwise, does not necessarily constitute or imply its endorsement, recommendation, or favoring by the United States Government or any agency thereof or its contractors or subcontractors. The views and opinions of authors expressed herein do not necessarily state or reflect those of the United States Government or any agency thereof.

Tandem Electrocatalytic-Thermocatalytic Conversion of CO_2 to Aromatic Hydrocarbons

Samay Garg[1,†], Zhenhua Xie[1,2,†], Alexandria X. Lam[1], Jingguang G. Chen[1,2,]*

1. Department of Chemical Engineering, Columbia University, New York, NY 10027, USA

2. Chemistry Division, Brookhaven National Laboratory, Upton, NY 11973, USA

† These authors contributed equally

* Corresponding author: jgchen@columbia.edu

Abstract

The reaction of CO_2 with H_2O to produce aromatic hydrocarbons (benzene, toluene, ethylbenzene, and xylene isomers) (BTEX) represents a promising pathway for converting CO_2 to value-added liquid products. However, this reaction cannot be achieved in a single electrochemical or thermochemical process. This work utilizes tandem electrochemical-thermochemical reactors as a new paradigm by starting with CO_2 and H_2O as the feed in a membrane electrode assembly (MEA) to produce C_2H_4, which subsequently undergoes thermochemical aromatization using a Gallium- and Phosphorus-modified zeolite ZSM-5 catalyst (Ga/ZSM-5/P) at ambient pressure to produce BTEX. The current study also demonstrates the potential advantage of the tandem strategy in mitigating negative effects of water by testing the tandem reactor system under different hydration conditions and by performing in-situ X-ray diffraction (XRD) and X-ray absorption (XAS) characterization of the aromatization catalysts. These results highlight the advantage of using the tandem process with the use of a water trap before the thermochemical reactor.

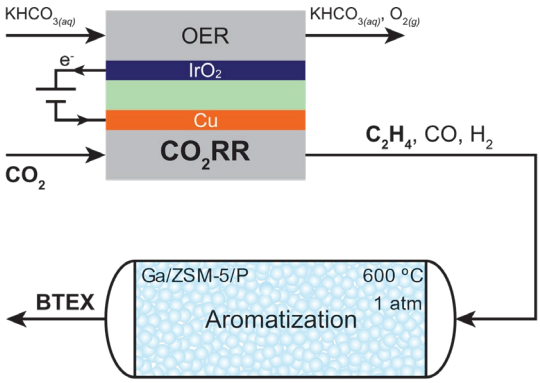

Anthropogenic greenhouse gas emissions have been linked to global temperature rise, ocean acidification, and other environmental imbalances. In order to limit global warming to 1.5° C above pre-industrial levels and avoid the worst effects of climate change, the Intergovernmental Panel on

Climate Change (IPCC) has called for reduction in greenhouse gas emissions by 45% compared to 2010 level by 2030, and net zero emissions by 20501. Achieving net zero emissions will require carbon utilization to close the carbon cycle and prevent carbon dioxide (CO2) from accumulating in the atmosphere, and utilizing CO2 as a C-atom feedstock for chemical manufacturing is one potential CO2 utilization strategy. Using CO2 for synthesizing high-volume commodity chemicals can also reduce the current reliance on fossil fuels for both material feedstocks and energy, which is critical as the chemical industry is considered a hard-to-abate sector2.

Effective catalysis is necessary to overcome the extraordinary stability of the C=O double bonds in CO_2 while minimizing the activation energy required for CO_2 conversion. Thermocatalytic CO_2 conversion is among the most widely studied approaches to CO_2 conversion, but these processes require large amounts of energy to generate the temperatures and pressures necessary for the reactions to proceed, as well as co-fed reducing agents that are often derived from fossil fuels, most notably hydrogen (H_2) produced by steam methane reforming. Electrocatalytic CO_2 conversion is a logical alternative that easily integrates with renewable energy; however, the practical implementation of the electrochemical CO_2 reduction reaction (CO_2RR) is limited by low selectivities and yields of multi-carbon products, resulting in significantly increased energy input to obtain the desired products[3]. Furthermore, converting CO_2 directly into complex molecules, regardless of the type of energy employed, is difficult due to the many different bond scission, electron transfer, and bond formation steps required to form molecules containing more than two carbon atoms.

To overcome these challenges, we propose a tandem reactor scheme for direct conversion of CO_2 into aromatic hydrocarbons that involves first electrochemically reducing CO_2 to produce ethylene (C_2H_4), which is directly fed into a thermochemical aromatization reactor operating at

ambient pressure to produce a mixture of benzene, toluene, ethylbenzene, and xylene isomers (BTEX). These compounds are a key component of the chemical manufacturing chain that are used to produce a wide range of products, including plastics, synthetic textiles, and medicines. BTEX is currently produced by recovering aromatic compounds from the reformate product of catalytic naphtha reforming in oil refineries, a process which requires large amounts of energy to both power the reactors and separate the desired aromatics products from the other components[2]. In comparison, the proposed tandem reactor scheme is a promising new route for BTEX synthesis that does not require fossil fuel inputs. The proposed tandem process employs electrochemical CO_2RR for the generation of the C_2H_4 intermediate in a process that easily integrates with renewable energy sources. Coupling electrochemical and thermochemical reactors in this manner is also more compatible with a distributed chemical economy, which reduces the safety risks, costs, and environmental impacts associated with transporting and storing intermediate chemicals.

Recent work from our group has demonstrated that the commercial implementation of hybrid electrochemical-thermochemical tandem processes for methanol and C_3 oxygenate synthesis can potentially achieve net-zero or even net-negative CO_2 emissions, assuming that sufficient renewable electricity is available to power these reactors[4,5]. Experimentally, our group has employed the tandem reactor scheme to demonstrate the production of C_3 oxygenates and carbon nanofibers[6,7]; other groups have recently demonstrated the production of C_4H_{10} and oxygenate products by using a similar tandem strategy[8,9]. In the current study, we demonstrate that electrochemical CO_2RR to produce C_2H_4 can be coupled with thermochemical C_2H_4 aromatization to produce BTEX in a tandem electrochemical-thermochemical reactor scheme. In addition, we use the CO_2 to BTEX reaction as a case study to demonstrate the advantage of the tandem scheme

in controlling the concentration of water vapor, which modifies the aromatization catalyst and is confirmed using in situ characterizeation techniques.

In the tandem process CO_2 is electrochemically reduced to produce C_2H_4 in a membrane electrode assembly (MEA) using Cu-based catalysts. The MEA studies were initially performed independently of the thermocatalytic reaction to understand the effects of different Cu oxidation states and CO_2 flow rates on the electrocatalytic activity and selectivity toward C_2H_4 production. The MEA was then coupled with a downstream thermochemical reactor using a Gallium- and Phosphorus-modified zeolite ZSM-5 (Ga/ZSM-5/P) catalyst that was identified to be effective for aromatization of C_2H_4 at ambient pressure[10]. The effect of water content was studied by either hydrating or drying the C_2H_4-rich stream between the MEA and thermochemical reactor. In situ characterization using X-ray absorption spectroscopy (XAS) and X-ray diffraction (XRD) was also performed to determine the corresponding structural changes in the Ga/ZSM-5/P catalyst and understand the effect of water vapor concentration on the aromatization reaction.

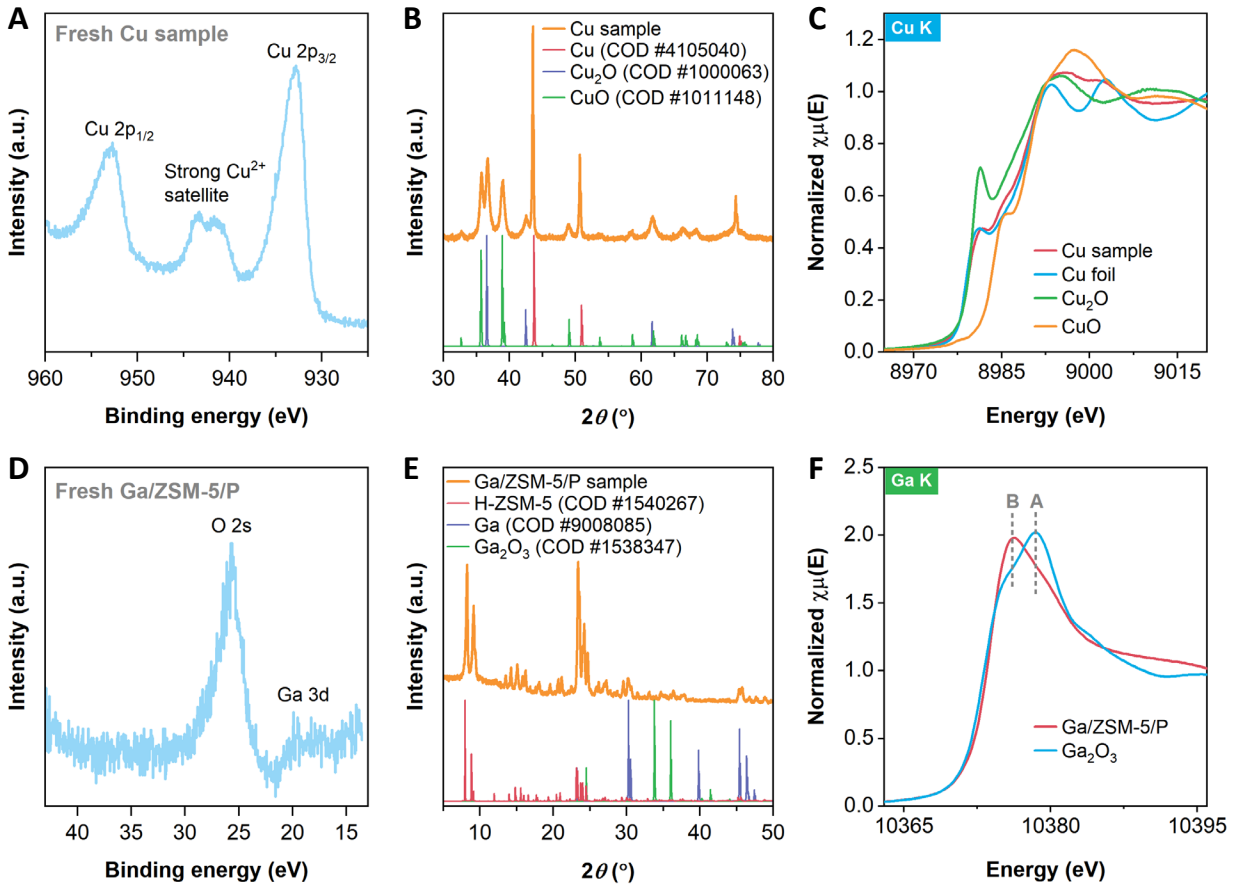

Figure 1. Characterization of the as-prepared Cu and Ga/ZSM-5/P catalysts used for the electrochemical and thermochemical reactors, respectively. (A) and (D) XPS plots of Cu 2p core level of the fresh Cu sample and Ga 3d level of the fresh Ga/ZSM-5/P sample, respectively; (B) and (E) XRD patterns of the Cu sample and the Ga/ZSM-5/P sample, respectively. (C) and (F) XANES plots of the Cu sample and the Ga/ZSM-5/P sample, respectively. Notes: For phase assignments, the simulated XRD patterns of referential standards (Cu, Cu_2O, CuO, Ga, α-Ga_2O_3, and H-ZSM-5) were also included; For comparison, the K-edge XANES spectra of standard compounds (Cu foil, Cu_2O, CuO, and Ga_2O_3) were also measured.

As illustrated in Figure 1, X-ray photoelectron spectroscopy (XPS) and X-ray diffraction (XRD) were employed to examine the near-surface chemical states and phase structure of the

representative Cu and Ga/ZSM-5/P catalysts. Figure 1A shows that, besides the satellite Cu^{2+} peak associated with CuO, two main broad and asymmetric peaks were observed at 932.9 eV (Cu $2p_{3/2}$) and 953.0 eV (Cu $2p_{1/2}$), close to that of Cu(0) and Cu_2O[11], suggesting the partial oxidation of the Cu sample. Although Cu and Cu_2O cannot be resolved based on the Cu $2p_{3/2}$ shifts due their closely similar binding energies (with only a 0.1 eV difference[11]), the XRD patterns (Figure 1B) corroborated the partial oxidation of Cu, along with the presence of Cu, Cu_2O and CuO, consistent with the partial oxidation feature as indicated by the X-ray absorption near-edge structure (XANES) spectrum (Figure 1C)[6]. Moreover, the XANES results indicated the dominance of the metallic Cu by the comparison with Cu foil, Cu_2O and CuO.

As for the fresh Ga/ZSM-5/P catalyst, the XPS signal of the Ga 3d level[12] (Figure 1D) was weak due to the relatively low loading of Ga (2 wt%) as well as the limited presence of Ga species on the external surface of the zeolite. Furthermore, despite the incorporation of Ga and P species, the MFI crystal structure of ZSM-5 was retained (Figure 1E). Notably, no diffraction peaks characteristic of metallic Ga and Ga_2O_3 were observed on the as-prepared sample, suggesting that the Ga species were highly dispersed on or within the zeolite. The Ga K-edge XAS was measured to probe the chemical state and local coordination environment of Ga in the Ga/ZSM-5/P sample. Ga_2O_3 powder was also measured as a reference standard for Ga^{3+}, and its XANES spectrum (Figure 1F) exhibited a prominent peak at 10378.5 eV (A) and a shoulder at 10376.2 eV (B). These two peaks corresponded to the presence of six- and four-coordinated Ga^{3+} species, respectively. The freshly calcined Ga/ZSM-5/P catalyst also displayed both characteristic peaks, but, with the dominance of the tetrahedral-associated peak. The extended X-ray absorption fine structure (EXAFS) results (see Figures 3B and 3D, Table S1) revealed the presence of shorter (d = 1.85 Å, average coordination number (CN) = 3.6) and longer (d = 2.02 Å, CN = 1.0) Ga-O bonds,

associated with the octahedral and tetrahedral GaO_x species, respectively. These CN_{Ga-O} values suggested that approximately 84% of the GaO_x species over the fresh catalyst were tetrahedral (see the calculations in SI). Moreover, a minor Ga-(O)-Ga bond associated with the GaO_x species was observed at 2.97 Å with a CN of ~0.3, consistent with the absence of diffraction patterns of Ga_2O_3.

Electrochemical CO_2RR was first assessed independently in a 5 cm^2 MEA to determine the conditions that would maximize C_2H_4 production. The effects of current density on cell voltage and C_2H_4 yield for each of the three Cu-based catalysts are shown in Figure 3, which compares the electrochemical performance and C_2H_4 yields for Cu, CuO, and Cu_2O with a CO_2 feed rate of 10 $ml \cdot min^{-1}$. Higher current densities favored increased ethylene yields for all catalysts; however, degradation of the MEA components caused significant instabilities in electrochemical performance at current densities greater than -200 $mA \cdot cm^{-2}$. Larger current densities correspond to higher overpotentials, which resulted in the observed increase in C_2H_4 yields[13]. Both copper oxides showed similar activity toward C_2H_4 production, while metallic Cu showed significantly higher C_2H_4 production. Although the reasons for this are not fully understood, it is likely a combination of morphological differences between the Cu oxides and Cu, as well as incomplete reduction of Cu oxide to metallic Cu under CO_2RR conditions. The maximum observed C_2H_4 yield was 23.1% at -250 $mA \cdot cm^{-2}$. Above -250 $mA \cdot cm^{-2}$, C_2H_4 activity began to decline as the effects of degradation of the MEA components became more pronounced, which was accompanied by an increase in H_2 production rates. Higher current densities also resulted in a greater amount of CO_2 crossover to the anode due to increased (bi)carbonate formation, with less than 20% of CO_2 fed to the reactor converted into gaseous CO_2RR products at -300 $mA \cdot cm^{-2}$, as shown in Figure S1.

Higher CO_2 feed rates and higher catalyst loadings were also tested in an attempt to increase C_2H_4 flow rates out of the MEA (see Figures S2-S3) by using 3 $mg \cdot cm^{-2}$ and 5 $mg \cdot cm^{-2}$ Cu

loadings for the cathode at a current density of -200 mA·cm^{-2}, as well as to enhance product flow rates at different current densities for the MEA with a Cu loading of 3 mg·cm^{-2}. In all cases, the C_2H_4 flow rate was lower than that of the benchmark MEA with a 1 mg·cm^{-2} Cu loading at a current density of -200 mA·cm^{-2}. Thus, a 1 mg·cm^{-2} cathode catalyst loading and a 10 mL·min^{-1} CO_2 feed were utilized for the subsequent tandem reactor experiments.

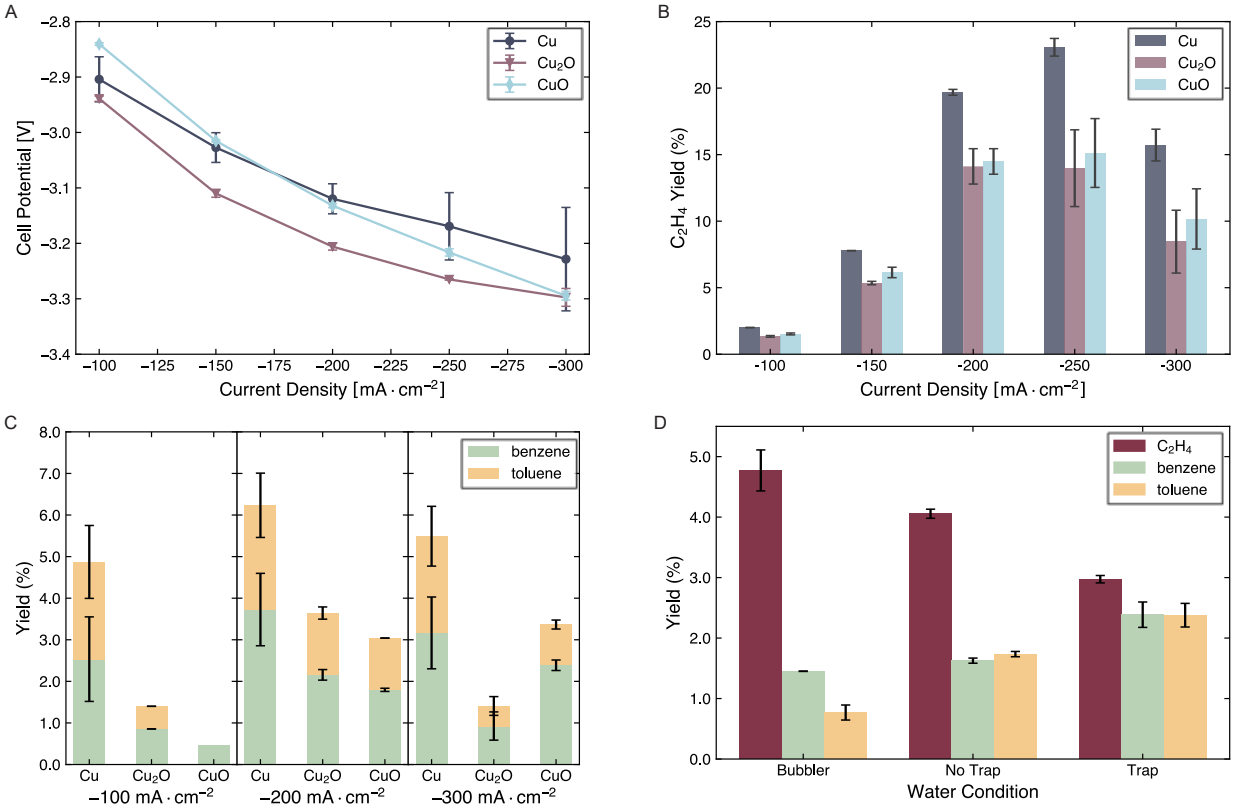

Figure 2. Catalytic performance within the individual electrochemical reactor (MEA) or the electrochemical-thermochemical tandem reactors. All experiments were conducted using a CO_2RR catalyst loading of 1 mg·cm^{-2}, CO_2 flow rate of 10 mL·min^{-1}, and 100 mg of Ga/ZSM-5/P. (A) Polarization curves measured using Cu, Cu_2O, or CuO as the cathode catalyst; (B) CO_2-based C_2H_4 yield from the MEA for each of the catalysts at different current densities; (C) CO_2-based selectivities for aromatic compounds at current densities from -100 mA·cm^{-2} to -300 mA·cm^{-2} using the three different Cu-based electrocatalysts in the CO_2RR MEA; (D) CO_2-based yield for

aromatic compounds and C_2H_4 after 70 min time on stream under different hydration conditions for the thermocatalytic reactor feed. Note: the reactor data in Figures 2C and 2D were obtained from the tandem reactor experiments

The CO_2RR electrolyzer was integrated with a downstream thermochemical aromatization reactor containing 100 mg of Ga/ZSM-5/P (2 wt% Ga, 0.8 wt% P) operating at 600 ºC and ambient pressure. The MEA outlet stream passed through a water trap before entering the inlet of the thermochemical reactor. The same three CO_2RR catalysts were tested, and the tandem system was also evaluated at progressively higher current densities.

The effect of current density on ultimate aromatics yield was tested, and the results are shown in Figure 2C. As expected, based on the higher C_2H_4 yields observed during the electrochemical reactor experiments, the tandem system using Cu as the CO_2RR catalyst showed the highest aromatics yield, with a maximum total aromatics yield of 6.2 % at -200 $mA \cdot cm^{-2}$. Although this yield seems modest, it is calculated based on the total CO_2 conversion, which includes CO_2 crossover to the anode in the form of (bi)carbonates and other liquid products that do not enter the thermochemical reactor. Notably, separating BTEX from the unreacted CO_2 and the side products of the thermochemical reaction, primarily ethane and C_3 hydrocarbons, is simple and requires minimal energy because the constituents of BTEX have relatively high boiling points compared to these other compounds and can therefore simply be condensed out of the reactor effluent to obtain a high purity product.

To fully understand the effect of residual water vapor from the electrochemical reactor on the thermocatalytic reaction, the tandem reactor was tested under three different operating conditions (Figure 2D): (1) the MEA output was fed directly into the thermochemical reactor with no intervening step, (2) a water trap submerged in an ice bath was inserted between the MEA and the

thermochemical reactor to dry the MEA output of residual water before entering the thermochemical reactor, and (3) a bubbler filled with de-ionized water was inserted between the MEA and the thermochemical reactor to feed excess water into the thermochemical reactor. These experiments were conducted using 10 mg of thermocatalyst in order to accelerate the water-poisoning of the catalyst and correlate the lab-scale reactor data with the in situ XAS data that will be discussed later.

There was a notable decrease in the total aromatics yield from 4.8% with the water trap to 2.2% with the bubbler, which underscores the deleterious effect residual water vapor has on the thermocatalyst. This reduction in performance was also reflected in the increased amount of unreacted C_2H_4 present in the product stream, with the C_2H_4 yield increasing from 3.0% with the water trap to 4.8% with the bubbler. The total aromatics yield also remained stable after 3 hours on stream (Figure S9), which highlights the stability of the tandem reactor system. XRD characterization (Figure S7) of spent Ga/ZSM-5/P catalyst samples revealed no change in the crystal structure of the catalyst, and thermogravimetric (TGA) analysis of these samples (Figure S8) showed that there was very little coke formation, both of which further confirm the stability of the Ga/ZSM-5/P catalyst.

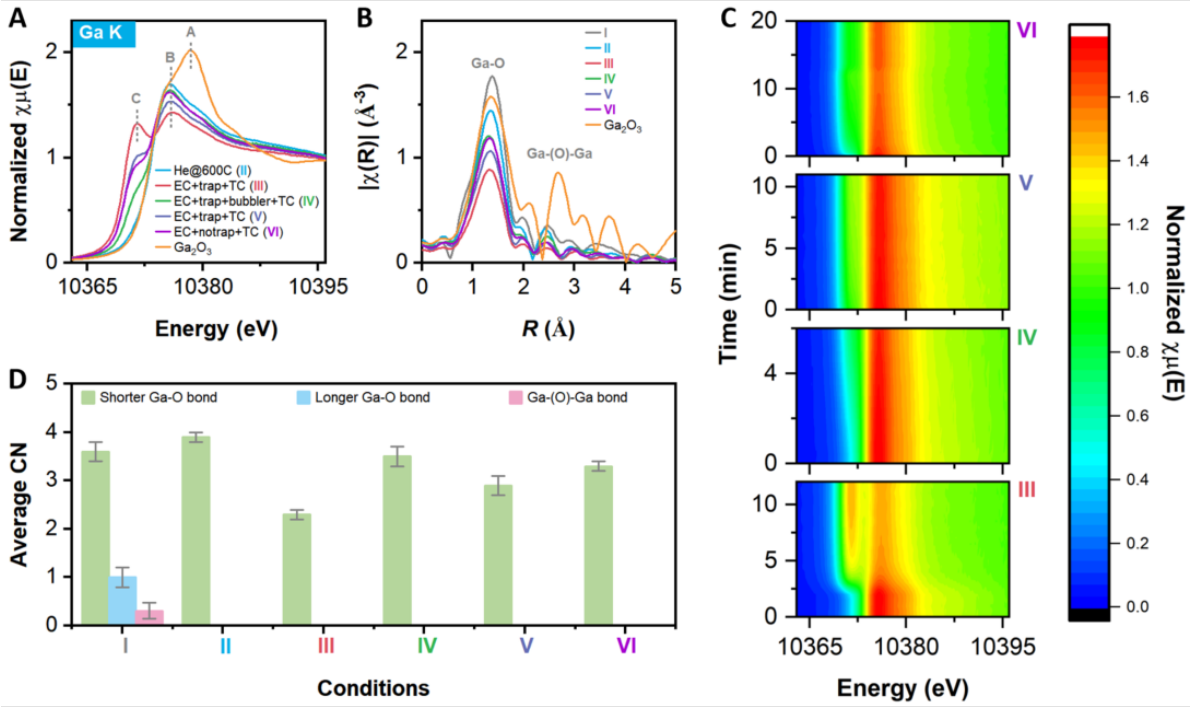

Figure 3. In situ Ga K-edge XAS results of Ga/ZSM-5/P under different conditions as well as Ga_2O_3. (A) XANES results; (B) EXAFS results in R space; (C) Time-resolved contour plots of normalized XANES spectra under different reaction conditions; (D) Average CN of chemical bonds under different conditions. Notes: I—treatment in Helium at 25°C; II—treatment in Helium at 600°C; III—tandem reactors with the configuration of elctrochemical reactor (MEA, 25°C)+water trap+thermochemical reactor (600°C); IV—elctrochemical reactor (MEA, 25°C)+water trap+water bubbler+thermochemical reactor (600°C); V—elctrochemical reactor (MEA, 25°C)+water trap+thermochemical reactor (600°C); VI—elctrochemical reactor (MEA, 25°C)+no water trap+thermochemical reactor (600°C). The XAS spectrum of "EC+notrap+TC (VI)" was collected immediately after the He pretreatment at 600°C using a fresh Ga/ZSM-5/P catalyst.

The evolution of chemical state and local coordination environment of Ga during the tandem process was examined under different conditions using in situ XAS at the Ga K-edge. The in situ experiments were performed using the same electrocatalytic-thermocatalytic configuration with approximately 10 mg of the Ga/ZSM-5/P catalyst. After a Helium treatment at 600°C (II), the minor Ga-(O)-Ga bond (d=2.97 Å, CN=~0.3) associated with the GaO_x species nearly disappeared, consistent with the previously reported redispersion of Ga species through migration into zeolite pores and ion exchange with Brønsted acid protons[14–16]. Accordingly, the CN of the Ga-O bond transformed to 3.9 with a bond length of 1.83 Å, corresponding to a four-fold coordination in the zeolite framework. The catalyst was subsequently subjected to a reaction stream from the cathode outlet of the MEA. It is noted that a water trap (III) was added between the MEA and the thermochemical reactor to remove water if any from the MEA. Figures 3A and 3C show that the Ga species underwent further reduction with a significant shift of the edge position towards lower energy; simultaneously, the $CN_{Ga\text{-}O}$ (Figure 3D) decreased from 3.9 after the 600°C Helium treatment to 2.3, suggesting coordination with two oxygen atoms from ZSM-5. Notably, a third resonance peak C (Figure 3A) was observed at the condition of III. Although both monovalent Ga^+ species and $[Ga(III)H_2]^+$ species likely exhibited the peak C feature due to their similar electronic structures, the latter was ruled out under the present reaction condition (600°C) since it typically becomes unstable at temperatures exceeding 500°C[15,17,18]. This is consistent with our previous density functional theory (DFT) calculations that a Brønsted−Lewis acid site pair with a Ga^+ species exhibited the lowest energy state over Ga/ZSM-5[10]. It served as the precursor of the active sites in ethylene aromatization, during which the adjacent Brønsted acid sites can protonate the Ga^+ site to form $[(Ga(III)H)]^{2+}$ or $[Ga(III)H_2]^+$ intermediate species, thereby increasing the Lewis acid strength and in turn facilitating the aromatization process such as the oligomerization

step[10,16,17]. The introduction of P has shown decreased barriers associated with benzene desorption and H_2 formation[10]. However, upon passing the cathode effluents through a water bubbler (IV), significant changes were immediately observed in both XANES (Figures 3A and 3C) and EXAFS (Figures 3B and 3D), indicating rapid oxidization of Ga by water vapor and an increase in CN_{Ga-O} from 2.3 to 3.5. This can be attributed to the strongly exothermic oxidation (e.g., ΔH = -197 kJ/mol)[14] of monovalent Ga^+ species by water molecules, forming $[Ga(III)(OH)_2]^+$ or Ga(III)OOH species; the subsequent dehydration is highly endothermic (e.g., ΔH = +302 kJ/mol)[14], leading to the poisoning of Lewis acid sites by water[10]. Indeed, subsequent bypassing the water bubbler (V) only partially restored the active sites with CN_{Ga-O} of ~2.9. Another control experiment without the water trap (VI) led to more oxidation feature of Ga compared to that with the water trap (III), consistent with its lower yield of aromatics (Figure 2D). Although the presence of P over the Ga/ZSM-5/P catalyst was reported to reduce water binding strength[10], it appeared insufficient to fully suppress the poisoning effect, particularly with excessive water vapor. These observations highlight the importance of removing water before entering the downstream thermocatalytic reactor for aromatization in the electrocatalytic-thermocatalytic tandem strategy. This also justifies the advantage of the tandem strategy over conventional one-pot thermocatalytic processes, wherein the in situ generated water is unavoidably introduced to the catalyst, potentially compromising its activity and yield.

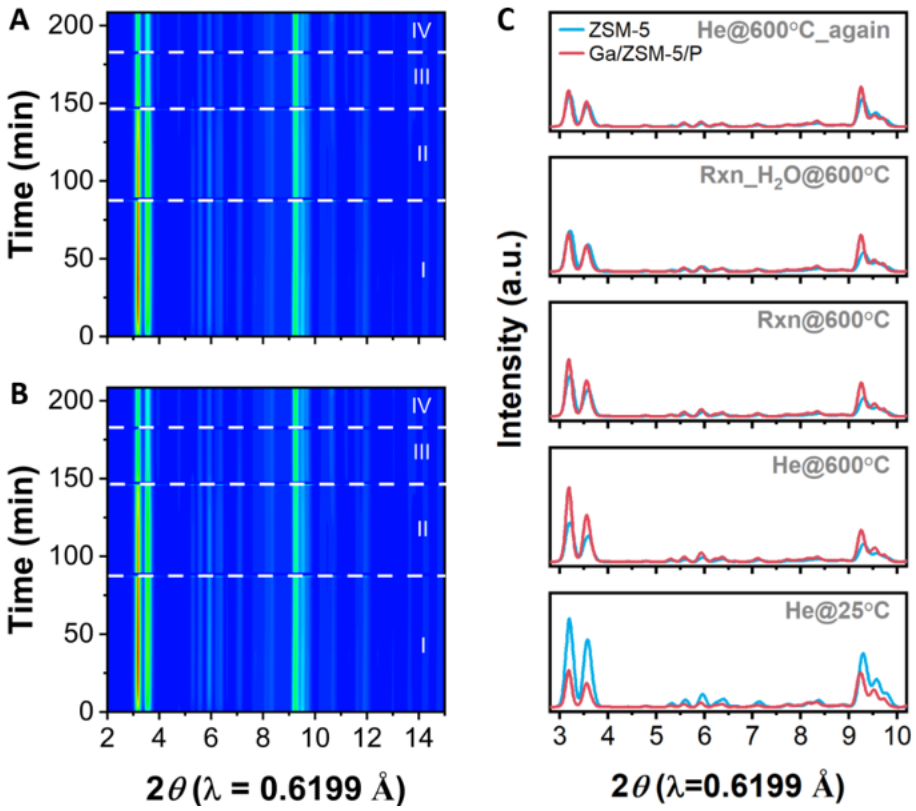

Figure 4. In situ XRD patterns of Ga/ZSM-5/P and ZSM-5 under different conditions. (A) Ga/ZSM-5/P; (B) ZSM-5; (C) Comparison of XRD patterns of Ga/ZSM-5/P and ZSM-5 at the steady state under different conditions. Notes: I: Helium (He), heating from room temperature to 600°C; II: C_2H_4/CO/He (Rxn), 600°C; III: C_2H_4/CO/H_2O/He (Rxn_H_2O), 600°C; IV: He, 600°C.

In situ XRD measurements were performed to further understand the phase structure and stability of the aromatization catalyst, Ga/ZSM-5/P, using feeds simulating those generated from the MEA cathode. Figures 4A-C show that the addition of Ga and P to ZSM-5 resulted in a weakening of diffraction peak intensities and a decrease in zeolite crystallinity compared to pure ZSM-5[19]. Upon activation at 600°C in Helium, ZSM-5 (Figure 4B) exhibited a notable decline in crystallinity due to the high-temperature treatment, while Ga/ZSM-5/P retained its crystallinity during activation and only gradually experienced reduced crystallinity during the aromatization

process. No diffraction peaks associated with the Ga phases (e.g., Ga_2O_3 and Ga) were observed in the Ga/ZSM-5/P catalyst (Figure 4A), verifying the high dispersion of Ga species on the surface or within the pore of the zeolite. The Ga/ZSM-5/P catalyst generally held a phase of P21/n space group (monoclinic) and the diffraction peaks appeared at lower 2θ angles (Figure 4C) than the pure ZSM-5 (Si/Al=30), consistent with lattice expansion by the incorporation of Ga ions into the zeolite framework as indicated by the EXAFS analysis. It is important to note that the P introduction did not induce structural transformation of ZSM-5 into silicoaluminophosphate-like structures.

In conclusion, this work has demonstrated a tandem electrochemical-thermochemical reactor paradigm for the synthesis of BTEX from CO_2. By connecting the output of a CO_2 electrolyzer with a Cu electrocatalyst for CO_2RR to the input of a thermochemical reactor operating at 600 ºC and ambient pressure with a Ga/ZSM-5/P catalyst, BTEX was obtained with a CO_2-based yield of 6.2%. In situ characterization under different hydration conditions for the feed to the thermochemical reactor provided further insights into the importance of reducing water vapor concentration to maintain the structures and chemical states of the aromatization catalysts. The results presented are a promising step forward in directly converting CO_2 to aromatic hydrocarbons at ambient pressure, which cannot be easily achieved using either electrocatalysis or thermocatalysis alone. Future work should be done to optimize the MEA stability and C_2H_4 yield and production rate to bring the system closer to commercial viability.

Supporting Information

Experimental methods; additional CO_2RR results; thermochemical reactor results; additional EXAFS characterization of Ga/ZSM-5/P; additional characterization of spent catalysts; additional tandem reactor results

Acknowledgements

This research was supported by the U.S. Department of Energy, Office of Basic Energy Sciences, Catalysis Science Program (Grant No. DE-FG02-13ER16381). This research used beamline 7-BM (QAS) of the National Synchrotron Light Source II (NSLS-II) at BNL (Contract No. DE-SC0012704) and was supported in part by the Synchrotron Catalysis Consortium (Grant No. DE-SC0012653). Samay Garg acknowledges support by the National Science Foundation Graduate Research Fellowship under Grant No. DGE-2036197.

References

(1) IPCC. Global Warming of 1.5°C: IPCC Special Report on Impacts of Global Warming of 1.5°C above Pre-Industrial Levels in Context of Strengthening Response to Climate Change, Sustainable Development, and Efforts to Eradicate Poverty, 1st ed.; Cambridge University Press, 2022. https://doi.org/10.1017/9781009157940.

(2) Technology Roadmap - Energy and GHG Reductions in the Chemical Industry via Catalytic Processes – Analysis. IEA. https://www.iea.org/reports/technology-roadmap-energy-and-ghg-reductions-in-the-chemical-industry-via-catalytic-processes (accessed 2022-09-25).

(3) Jeng, E.; Jiao, F. Investigation of CO2 Single-Pass Conversion in a Flow Electrolyzer. React. Chem. Eng. **2020**, 5 (9), 1768–1775. https://doi.org/10.1039/D0RE00261E.

(4) Biswas, A. N.; Winter, L. R.; Xie, Z.; Chen, J. G. Utilizing CO2 as a Reactant for C3 Oxygenate Production via Tandem Reactions. JACS Au **2023**, 3 (2), 293–305. https://doi.org/10.1021/jacsau.2c00533.

(5) Tackett, B. M.; Gomez, E.; Chen, J. G. Net Reduction of CO2 via Its Thermocatalytic and Electrocatalytic Transformation Reactions in Standard and Hybrid Processes. Nat. Catal. **2019**, 2 (5), 381–386. https://doi.org/10.1038/s41929-019-0266-y.

(6) Biswas, A. N.; Xie, Z.; Xia, R.; Overa, S.; Jiao, F.; Chen, J. G. Tandem Electrocatalytic–Thermocatalytic Reaction Scheme for CO2 Conversion to C3 Oxygenates. ACS Energy Lett. **2022**, 7 (9), 2904–2910. https://doi.org/10.1021/acsenergylett.2c01454.

(7) Xie, Z.; Huang, E.; Garg, S.; Hwang, S.; Liu, P.; Chen, J. G. CO2 Fixation into Carbon Nanofibres Using Electrochemical–Thermochemical Tandem Catalysis. Nat. Catal. **2024**, 7 (1), 98–109. https://doi.org/10.1038/s41929-023-01085-1.

(8) Zhang, J.; Kang, X.; Yan, Y.; Ding, X.; He, L.; Li, Y. Cascade Electrocatalytic and Thermocatalytic Reduction of CO2 to Propionaldehyde. Angew. Chem. **2024**, 136 (12), e202315777. https://doi.org/10.1002/ange.202315777.

(9) Lee, M. G.; Li, X.-Y.; Ozden, A.; Wicks, J.; Ou, P.; Li, Y.; Dorakhan, R.; Lee, J.; Park, H. K.; Yang, J. W.; Chen, B.; Abed, J.; dos Reis, R.; Lee, G.; Huang, J. E.; Peng, T.; Chin, Y.-H. (Cathy); Sinton, D.; Sargent, E. H. Selective Synthesis of Butane from Carbon Monoxide Using Cascade Electrolysis and Thermocatalysis at Ambient Conditions. Nat. Catal. **2023**, 6 (4), 310–318. https://doi.org/10.1038/s41929-023-00937-0.

(10) Gomez, E.; Nie, X.; Lee, J. H.; Xie, Z.; Chen, J. G. Tandem Reactions of CO2 Reduction and Ethane Aromatization. J. Am. Chem. Soc. **2019**, 141 (44), 17771–17782. https://doi.org/10.1021/jacs.9b08538.

(11) Ghodselahi, T.; Vesaghi, M. A.; Shafiekhani, A.; Baghizadeh, A.; Lameii, M. XPS Study of the Cu@Cu2O Core-Shell Nanoparticles. Appl. Surf. Sci. **2008**, 255 (5, Part 2), 2730–2734. https://doi.org/10.1016/j.apsusc.2008.08.110.

(12) Uslamin, E. A.; Luna-Murillo, B.; Kosinov, N.; Bruijnincx, P. C. A.; Pidko, E. A.; Weckhuysen, B. M.; Hensen, E. J. M. Gallium-Promoted HZSM-5 Zeolites as Efficient Catalysts for the Aromatization of Biomass-Derived Furans. Chem. Eng. Sci. **2019**, 198, 305–316. https://doi.org/10.1016/j.ces.2018.09.023.

(13) Kuhl, K. P.; Cave, E. R.; Abram, D. N.; Jaramillo, T. F. New Insights into the Electrochemical Reduction of Carbon Dioxide on Metallic Copper Surfaces. Energy Environ. Sci. **2012**, 5 (5), 7050–7059. https://doi.org/10.1039/C2EE21234J.

(14) Kazansky, V. B.; Subbotina, I. R.; van Santen, R. A.; Hensen, E. J. M. DRIFTS Study of the Nature and Chemical Reactivity of Gallium Ions in Ga/ZSM-5: II. Oxidation of Reduced Ga Species in ZSM-5 by Nitrous Oxide or Water. J. Catal. **2005**, 233 (2), 351–358. https://doi.org/10.1016/j.jcat.2005.05.004.

(15) Kazansky, V. B.; Subbotina, I. R.; van Santen, R. A.; Hensen, E. J. M. DRIFTS Study of the Chemical State of Modifying Gallium Ions in Reduced Ga/ZSM-5 Prepared by Impregnation: I. Observation of Gallium Hydrides and Application of CO Adsorption as a Molecular Probe for Reduced Gallium Ions. J. Catal. **2004**, 227 (2), 263–269. https://doi.org/10.1016/j.jcat.2004.07.021.

(16) Zhou, Y.; Thirumalai, H.; Smith, S. K.; Whitmire, K. H.; Liu, J.; Frenkel, A. I.; Grabow, L. C.; Rimer, J. D. Ethylene Dehydroaromatization over Ga-ZSM-5 Catalysts: Nature and Role of Gallium Speciation. Angew. Chem. Int. Ed. **2020**, 59 (44), 19592–19601. https://doi.org/10.1002/anie.202007147.

(17) Schreiber, M. W.; Plaisance, C. P.; Baumgärtl, M.; Reuter, K.; Jentys, A.; Bermejo-Deval, R.; Lercher, J. A. Lewis–Brønsted Acid Pairs in Ga/H-ZSM-5 To Catalyze Dehydrogenation of Light Alkanes. J. Am. Chem. Soc. **2018**, 140 (14), 4849–4859. https://doi.org/10.1021/jacs.7b12901.

(18) Hensen, E. J. M.; García-Sánchez, M.; Rane, N.; Magusin, P. C. M. M.; Liu, P.-H.; Chao, K.-J.; van Santen, R. A. In Situ Ga K Edge XANES Study of the Activation of Ga/ZSM-5 Prepared by Chemical Vapor Deposition of Trimethylgallium. Catal. Lett. **2005**, 101 (1), 79–85. https://doi.org/10.1007/s10562-004-3753-x.

(19) Choudhary, V. R.; Devadas, P.; Banerjee, S.; Kinage, A. K. Aromatization of Dilute Ethylene over Ga-Modified ZSM-5 Type Zeolite Catalysts. Microporous Mesoporous Mater. **2001**, 47 (2), 253–267. https://doi.org/10.1016/S1387-1811(01)00385-7.